Desalination and Water Treatment
www.deswater.com

doi: 10.5004/dwt.2021.26578

210 (2021) 296–308
January

Synthesis of zeolite from fly ash: application to adsorption of COD from cheese whey wastewater

Naghme Helali[a], Erfan Shabani[b], Puria Heidarian[c], Farhad Salimi[d,*]

[a]*Department of Food Industry Engineering, Ayatollah Amoli Branch, Islamic Azad University, Amol, Iran, email: helali22@yahoo.com (N. Helali)*
[b]*Department of Food Industry Engineering, Varamin Pishva Branch, Islamic Azad University, Tehran, Iran, email: erfunshabani@gmail.com (E. Shabani)*
[c]*Department of Chemical Engineering, Isfahan University and Technology, Isfahan, Iran, email: puria_92@yahoo.com (P. Heidarian)*
[d]*Department of Chemical Engineering, Kermanshah Branch, Islamic Azad University, Kermanshah, Iran, email: f.salimi@iauksh.ac.ir (F. Salimi)*

Received 18 April 2020; Accepted 13 September 2020

ABSTRACT

In this study, raw fly ash (RFA) was used to synthesize zeolite (the zeolitized fly ash, ZFA) via a two-step process (alkaline fusion-hydrothermal synthesis). RFA and ZFA were characterized by X-ray fluorescence, X-ray diffraction, scanning electron microscopy, and Fourier transform infrared. The prepared ZFA was employed as the adsorbent in the batch adsorption of chemical oxygen demand (COD) from cheese whey wastewater. The effect of operational parameters on the adsorption process was investigated. The results showed that the adsorption efficiency increases with the increase of pH, contact time, adsorbent dosage, and temperature. The optimum conditions were determined as pH of 11, a contact time of 20 min (q_e = 330.088 mg/g), and adsorbent dosage of 0.4 g for COD adsorption on ZFA. Kinetic analysis of the COD adsorption on ZFA indicated that the adsorption process was controlled by the Morris–Weber-order model. Moreover, the isotherm models were subjected to the experimental data of the COD adsorption on ZFA. The results revealed that the COD adsorption on ZFA involved physical adsorption with good adsorption characteristics. The calculated values of the thermodynamic parameters such as $\Delta H°$, $\Delta S°$, and $\Delta G°$ revealed that the adsorption of COD on ZFA was feasible, spontaneous, and endothermic. In fact, high adsorption efficiency can be obtained in a short time using ZFA as the adsorbent for the COD removal from cheese whey wastewater.

Keywords: Adsorption; COD; Cheese whey wastewater; Raw fly ash; Synthetic zeolite

1. Introduction

Dairy effluents include wastewater from dairy products, namely ice cream, cheese, and yogurt, as well as wastewater from washing the halls and production line equipment. The intensity of contamination and the wastewater volume of each dairy factory depends on the volume of the processed milk, product type, conditions sand type of equipment, production method, system management, and system washing program [1]. The entry of untreated wastewater into the environment makes unsightly landscapes and causes unpleasant odors in the surrounding environment of the factory in addition to creating pollution and health hazards.

Many techniques have been introduced to remove contaminants from wastewaters. Biological, oxidation or

* Corresponding author.

ozonation [2,3], flocculation [4], membrane separation [5], and adsorption [6,7].

One of the methods employed to eliminate metal and organic contaminants from water is the use of adsorbents for the adsorption method [8–11]. Elimination by adsorption includes the adhesion of soluble and suspended pollutants to an organic or mineral solid. This binding of the contaminant to the adsorbent depends on the structure and composition of the contaminant and the nature of the adsorbent. This process is affected by the electrostatic and van der Waals forces as well as phenomena such as ion exchange and complex formation. The elimination of pollutants from wastewater is affected by several factors, namely the adsorption level, pH, particle size, contact time, temperature, and presence of salt and metal. Absorption is a non-selective process. Therefore, other compounds in wastewater can be absorbed by the adsorbent, thus reducing the adsorption capacity [12].

Adsorbents can be organic or mineral. Mineral adsorbents are superior to organic adsorbents in terms of mechanical resistance, chemical stability, specific surface area, and stability facing microbial decomposition. Compounds like activated carbon, natural zeolites, bentonite, chitosan, corn wood, rice husk, barley bran, and dried activated sludge have been employed as adsorbents [13–17].

Zeolites have cations of alkali and alkaline earth metals and also an unlimited structure. Zeolites are hydrated aluminum silicate crystals with the cations of alkali and alkaline earth metals. They have an infinite structure and their characteristics include cation-exchange, reversibility, water uptake, and excretion without significant changes in their molecular structure. Natural zeolites typically hold a negative electric charge on their surface, thus having the ability to exchange cations [18]. The physical and chemical properties of natural zeolites vary, insofar as there are differences in the physical properties (namely the cavity size, crystal size, ion exchange capacity, and adsorption capacity) and the chemical mixture among various samples of a distinct type of zeolite [19].

The synthesis of silicon and aluminum in fly ash was activated by fusion with sodium carbonate in the study by Yaping et al. [20]. They extracted the silicon and aluminum from the ash via fusing it with sodium carbonate. Then, this mixture was used to make various zeolites in pure form. The synthesized samples were tested in terms of mineral and crystalline composition and cation exchange capacity (CEC). The results revealed that the pure zeolites produced had a high CEC in the range of 2.6–3.4 meq/g.

Ríos et al. [21] compared two methods of synthesizing sodium and potassium zeolites produced from fly ash. In this research, the desired zeolites were made throughout hydrothermal operations in NaOH and KOH alkaline mixtures. The results revealed that the type of the created zeolite changed with the operational conditions. In addition, the examination of the zeolites created for their CEC confirmed that these zeolites, which were made from ash, could absorb heavy metals, and were employed in water and wastewater treatment operations. Belviso et al. [22] conducted studies about the formation of zeolite from Italian coal. The main objective of their study was to investigate the differences in the crystallization temperatures when seawater was employed instead of distilled water. The results confirmed that in such a scenario, X and ZK-5 zeolites were synthesized at lower temperatures (35°C and 45°C). Shoumkova and Stoyanova [23] conducted a study on the creation of different zeolites by the alkaline hydrothermal process on the coal fly ash from the thermal power station. In this work, fly ash from lignite coal fuel underwent the hydrothermal activation process with KOH and NaOH at various temperatures to form different zeolites. The results indicated that activation with KOH (>6 M) and NaOH (>3 M) for 7 h at 393°C–373°C resulted in the production of Linde F and hydroxy sodalite, respectively. Zeolites have been employed to eliminate water pollutants, namely phenol, chlorophenol, dye, and *p*-nitrophenol [17,24–26].

Recently, Oliveira et al. [27] synthesized zeolite from sugarcane bagasse fly ash and used it as a low-cost adsorbent to remove heavy metals. They understood the temperature and the calcination time are key parameters affecting the ion-exchange capacity (q) of the zeolitic materials. Calcination at 600°C for 8 h, under an oxygen atmosphere, ensures that all the carbon from fly ash has been removed, and optimizes the ion exchange properties.

In this work, ZFA (zeolitized fly ash) was synthesized via the crystallization process. The ZFA structure was analyzed by X-ray diffraction (XRD), scanning electron microscopy (SEM), and Fourier transform infrared (FTIR) analyzes and used in batch experiments as an adsorbent to adsorb COD from whey effluent. The optimal conditions for chemical oxygen demand (COD) adsorption by ZFA were examined using parameters such as pH, contact time, adsorption, and temperature. Moreover, the kinetics of adsorption, adsorption isotherms, and thermodynamic parameters of the COD adsorption process were examined using zeolite.

2. Material and methods

2.1. Introduction

The present paper included two steps: the first step was the synthesis of ZFA from raw fly ash (RFA) and the second was using the synthetic zeolite for COD adsorption from whey water. In this section, the material and equipment for zeolite synthesis, synthesis method, physico-chemical characteristics of the adsorbent, adsorption test methods in the batch system, and materials and methods used in the tests are reviewed.

2.2. Materials and instruments

The main feed is RFA which is prepared from the chimney of Alborz Sharghi coal factory located in shahroud. Sodium hydroxide tablet (NaOH), sodium aluminate ($NaAlO_2$), deionized distilled water all were prepared from Merck Company (Germany). Cheese whey wastewater of PEGAH diary factory was used in this work.

To determine the crystal structure, degree of crystallinity, and existence of phases, XRD analysis was employed and this analysis was accomplished with the GBC X-ray diffractometer. In this device, the sample was exposed to XRD with 2θ angle between 5° and 80°. Scanning was performed continuously with 40 kV and 30 mA. Morphology and surface

structure of ZFA was determined by Deutschland Philips SEM XL30. Before using SEM, the surface was gold-coated with a sputter for better conduction and high-quality imaging. The functional group was determined by Vertex FTIR (Bruker, Germany). At the end, to measure the COD concentration in cheese whey wastewater, a spectrophotometer (catalog no. 114555 manual Photometer SQ300 Merck (was used. In order to the characterization of zeolite elemental mixture X-ray fluorescence (XRF) spectroscopy was used. Then XRF which is a semi-quantitative analysis tool was used to determine the chemical composition, whereas the major mineral phase was identified using the XRD technique.

2.3. ZFA synthesis

First, 10 g of RFA was mixed with 12 g of NaOH (1.2:1 w/w ratio) in a ball mill. Then, the mixture was melted in a furnace at 550°C (alkaline melting step). After 1 h in the furnace, the mixture was cooled at the room temperature and, then, was milled by a pounder to form a soft powder with extremely fine grains. After that, 2.87 g of sodium Aluminate (based on the ratio of $SiO_2/AL_2O_3 = 1$) and 100 mL of distilled water was added to the mixture. Then the mixture was mixed on a magnetic mixer in the room temperature for 16 h in order to obtain a homogeneous gel. In the last step, which was the hydrothermal step, the homogeneous gel was poured into an autoclave (because hydrothermal synthesis should be performed at high pressure and temperature) and the autoclave was put in an oven for 7 h at 100°C for the crystallization and formation of the desired ZFA. Then, the product, which was a suspension, was filtered by a filter paper and the remaining solid, which was ZFA, was washed with deionized water and, then, dried in the oven for 16 h at 105°C.

2.4. Test methods

All of the adsorption tests were done as a batch. The initial concentration of COD in cheese whey wastewater was 2,600 mg/L. In each test, the pH of the solution was adjusted by HNO_3 (1 M concentration) and NaOH (1 M concentration) solutions using a pH meter device.

In order to determine the optimal conditions in adsorption processes, at the first step, the pH should be optimized. For this purpose, 50 mL of COD solution with an initial concentration of 2,600 mg/L and 0.4 g of adsorbent was added to 11 separate Beaker. Different pH values in the 2–12 range were adjusted. After optimum pH measuring, for determining the optimum contact time, 0.4 g of adsorbent was added to wastewater with 2,600 mg/L initial concentration and at the optimum pH value, the solution was put on a mixer with 400 rpm rotation. After the beginning of the adsorption, the sample was taken at 2–22 min intervals. In each sample, the solution and the adsorbent were immediately separated by filtration and the solution was prepared for analysis. To determine the optimum adsorbent dosage and temperature in COD adsorption, the experiments were done in the range of 0.05–0.45 g and temperatures of 25°C, 35°C, and 45°C, respectively.

Following each test, the solution and the adsorbent were separated by a centrifuge and the solution was prepared for determining the COD concentration. Each sample was repeated twice and their results were compared to prevent errors. The error of tests was below 4%. The COD adsorption efficiency in each excrement can be calculated by Eq. (1):

$$\%\text{Removal efficiency} = \frac{\left(C_i - C_f\right)}{C_i} \times 100 \tag{1}$$

where C_i (mg/L) is the initial concentration of COD and C_f (mg/L) is the final concentration of COD in the cheese whey wastewater. Eq. (2) expresses the adsorbed COD by the adsorbent in t time:

$$q_t = \frac{V\left(C_0 - C_t\right)}{m} \tag{2}$$

where q_t (mg/g) is the adsorbed amount per gram of adsorbent, C_0 and C_f the concentrations of the dye in the initial (time of 0) and final (time of t) solution, respectively (mg/L); V the volume of the dye solution added (L); and m the amount of the adsorbent used (g). A equation similar to Eq. (2) is used for calculating of adsorbed COD by the adsorbent in the equilibrium:

$$q_e = \frac{V\left(C_0 - C_e\right)}{m} \tag{3}$$

where q_e (mg/g) is the adsorption capacity of COD in the equilibrium and C_e (mg/L) is the concentration of COD in the equilibrium.

The PZC was calculated using the following method: first, to completely remove the CO_2 dissolved in the water, 100 mL of deionized water was added to an Erlenmeyer flask capped with cotton and then was heated for 20 min. Next, 10 mL of it was added into 25 mL Erlenmeyer flask with 0.5 g of adsorbent and mixed for 24 h at 25°C. Finally, the solution pH indicates the PZC. This method has shown satisfactory results elsewhere [28–30].

2.5. Adsorption isotherms

The Langmuir surface adsorption isotherm which is obtained based on the argument consideration has the following assumptions:

- Adsorption sites on the adsorbent surface are uniform and all of them have the same adsorption strength.

In other words adsorption energy is the same and does not depend on the quantity of adsorbate and adsorption ability of all of the sites is the same and adsorbate quantity in each site has no effects on other sites.

- Adsorption bonds are reversible.
- The adsorbate thickness is just one molecule; it means that adsorption is monolayer [31].

So, generally Langmuir equation is expressed as:

$$\frac{C_e}{q_e} = \frac{1}{q_0 K_L} + \frac{1}{q_0} C_e \tag{4}$$

where q_e (mg/g) is the quantity of adsorbate per adsorbent mass in equilibrium, C_e (mg/L) is the equilibrium concentration, q_0 (mg/g) is the maximum quantity of adsorbate on adsorbent, and K_L (L/mg) is the Langmuir constant.

For Langmuir isotherm a dimensionless constant, R_L, is also defined that type of adsorption process can be predicted considering its value. If $R_L > 1$ process is unfavorable, if $R_L = 1$ process is linear, if $0 < R_L < 1$ process is favorable and if $R_L = 0$ process is irreversible. The equation of dimensionless R_L is given by Eq. (5) [32]:

$$R_L = \frac{1}{1 + K_L C_0} \tag{5}$$

where K_L is the Langmuir constant and C_0 is the smallest quantity of solution initial concentration.

The Langmuir isotherm was introduced assuming uniformity of the adsorbent surface sites and identical adsorption energy in these sites; but, indeed adsorption in different sites could change because real surfaces are not uniform. In Freundlich isotherm, it is assumed that adsorption surface sites are not uniform and have different adsorption energy. In fact, the Freundlich theory assumes a logarithmic decrease of enthalpy with the increase of the occupied sites. Freundlich equation has no theoretical basis and is based on the experimental data. This equation is expressed as follows [31]:

$$q_e = K_F \left(C_e\right)^{\frac{1}{n}} \tag{6}$$

where q_e and C_e have previous definition and K_F and $(1/n)$ are constants. K_F depends on adsorption capacity and $1/n$ indicates the rate of adsorption. n gives data about the nature of the adsorption process. $2 < n < 10$ shows desirable and good adsorption characteristics, $1 < n < 2$ shows partly weak adsorption characteristics and $n < 1$ indicates weak or undesirable adsorption characteristics.

The Temkin model includes a factor that completely expresses interactions between the adsorbent and the adsorbate. This model is based on the following assumptions and conditions:

- Adsorption heat of all of the molecules in a layer decreases linearly and simultaneously by the coating of the layer with molecules and this phenomenon occurs because of the adsorbent and the adsorbate interactions.
- In this model, to determine and interpret the adsorption, a uniform distribution of bond energies to the maximum bond energy process is employed.

According to the Temkin model, adsorption heat is linear rather logarithmic. Temkin model isotherm usually is expressed as Eq. (7) [33]:

$$q_e = B \ln\left(K_T C_e\right) \tag{7}$$

where $B = (RT/A_T)$ and K_T are Temkin constants, A_T (J/mol) is Temkin adsorption energy difference between two adjacent sits, T (K) is adsorption temperature, and R (kJ/mol K) is gas constant.

For better depict of diagrams and calculating Temkin constant linearized form of the equation is as:

$$q_e = B \ln\left(K_T\right) + B \ln\left(C_e\right) \tag{8}$$

Values of K_T and B are obtained from q_e and $\ln(C_e)$ linear diagram.

The Dubinin–Radushkevich model is usually used to evaluate the porosity and adsorption free energy. In this model, it is assumed that adsorption porosity curves are related to adsorbent porosity Dubinin assumes that the adsorption process is accomplished in the adsorbent cavity volume, which is in contrast with the layer-to-layer adsorption theory. Also, the Dubinin–Radushkevich model can be used for the determination of adsorption reaction nature (physical or chemical). Eq. (9) expresses this model [34,35]:

$$q_e = q_0 e^{-\beta\varepsilon^2} \tag{9}$$

Linearized form is as below:

$$\ln q_e = \ln q_0 - \beta\varepsilon^2 \tag{10}$$

where q_e (mg/g) is the equilibrium adsorption capacity, q_0 (mg/g) is monolayer adsorption capacity (maximum theoretical adsorption capacity), β (mol^2/kJ^2) is porosity factor, and ε is Polanyi potential which is defined as Eq. (11):

$$\varepsilon = RT \ln\left[1 + \frac{1}{C_e}\right] \tag{11}$$

where R (kJ/mol K) is gas constant, T (K) is temperature, and C_e (mg/L) is equilibrium capacity. By drawing $\ln(q_e)$ vs. ε^2 diagram one can calculate β and q_0 from slope and intercept.

Adsorption free energy (E) is defined as a change in free energy of one mole of the ion when it moves from the solution to the surface of the adsorbent.

The equation of free energy (E) is defined as follows:

$$E = \left(2\beta\right)^{-\frac{1}{2}} \tag{12}$$

where β is the Dubinin–Radushkevich equation constant. The value of E shows the nature of adsorption. If $E < 8$ kJ/mol adsorption is physical, if 8 kJ/mol $< E <$ 16 kJ/mol adsorption is chemical with ion exchange and if 20 kJ/mol $< E <$ 40 kJ/mol adsorption is chemical [36].

2.6. Adsorption kinetics

Solids adsorption process from water occurs in several steps and the overall adsorption process can be controlled using one or many of these steps. The first step includes adsorbate diffusion from solution to the external surface of the adsorbent. Hole diffusion is the second step and if this step is controlling one can investigate this phenomenon with the Weber–Morris equation. The third step is adsorbent surface diffusion. Generally, the third step implies that the final

equilibrium occurs according to an extremely low concentration of the adsorbate in the solution and a decline in the adsorbent's active sites.

In pseudo-first-order and pseudo-second-order kinetic models chemical reaction step controls adsorption operation. In many studies, these two equations are used in parallel and one of them has more agreement with experimental data. Pseudo-first-order equation is as follows:

$$\ln\left(q_e - q_t\right) = \ln\left(q_e\right) - k_1 \cdot t \tag{13}$$

where q_e (mg/g) and q_t (mg/g) are the amount adsorption capacities at the equilibrium and time t (min), respectively. In Eq. (13), t (h) is time, and k_1 (1/min) is the pseudo-first-order-equation constant. The pseudo-second-order equation is defined based on equilibrium capacity in which vehemence of site filling is assumed proportional with square of number of empty sites. Pseudo-second-order equation is defined as below [37]:

$$\frac{dq_t}{dt} = k_2\left(q_e - q_t\right)^2 \tag{14}$$

After integrating:

$$\frac{t}{q_t} = \frac{1}{k_2\left(q_e\right)^2} + \frac{t}{q_e} \tag{15}$$

In Eq. (15), t (min) is time, and k_2 (g/mg/h) is the pseudo-second-order equation constant. k_2 and q_e parameters are obtained from linear diagram of (t/q_t) vs. t.

It is generally difficult to distinguish between a process controlled by diffusion resistance or controlled by a chemical reaction. One of the methods that can be used for this purpose is the Morris–Weber equation presentation, which is as follows [38]:

$$q_t = k_{\text{id}} \cdot t^{0.5} + C \tag{16}$$

In this Eq. (16), q_t (mg/g) is adsorption capacity, k_{id} (mg/(g h)$^{1/2}$) is internal diffusion vehemence constant and C (mg/g) is the constant of boundary layer thickness. If q_t vs. $t^{0.5}$ diagram is linear, the process is controlled by diffusion resistance.

3. Results and discussion

RFA chemical composition is presented in Table 1. As it shows the main elements in RFA are Si, O, Al, Ca, Fe, Mg, and slight quantities of S, Na, K, and Li. It has been reported that RFA regardless of the type of coal has many chemical compositions [39]. According to ASTM C618 standard RFA in this paper is from type *F* ash. Type *F* ash is obtained from bituminous anthracite coal and contains silica and alumina materials. Also, this type of RFA has at least 70% weight of SiO_2, Al_2O_3, and Fe_2O_3 in its chemical composition [40]. Used RFA in this work according to XRF analysis shown in Table 1 has 84.68% weight of SiO_2, Al_2O_3, and Fe_2O_3 compounds.

3.1. Analysis of the adsorbents crystal structure by XRD

XRD pattern of used RFA in this paper is shown in Fig. 1. As it shows, the main crystal phase in RFA is related to quartz (SiO_2) and also kalium (CaO), hematite (Fe_2O_3), anhydrite ($CaSO_4$), and magnetite (Fe_3O_4) phases are present in the structure of adsorbent. Aluminum crystal phases like mullite could not be seen in the XRD pattern. However, according to the XRF analysis in Table 1, RFA has a 28/73% weight aluminum compound (Al_2O_3). This can be explained by the point that the elemental and chemical compound of RFA originates from the minerals of the initial coal, but the mineralogical structure and crystal phases of RFA are related to the furnace design and, generally, the coal combustion operation [41].

Fig. 2 indicates the XRD diagram related to ZFA which was made from RFA. All of the peaks in this Fig. 2 are related to merlinoite zeolite with $Na_{0.55}K_{4.21}Ca_{1.49}Ba_{0.43}$ $(H_2O)_{22.74}$ $[Si_{22.69}Al_{9.31}O_{64}]$ formula. This phenomenon showed that in the synthesis of ZFA from the RFA operation during the hydrothermal crystallization process, merlinoite zeolite had been made purely [42,43].

3.2. Analysis of adsorbents morphology by SEM

The RFA surface morphology is shown in Fig. 3. In this Fig. 3, the non-porous and irregular structure of ash is observed. The morphology of the ZFA surface is shown in Fig. 4. As can be seen, the ZFA grain structure is obvious and, according to the literature, this kind of structure is expected [44].

3.3. Effect of pH on the analysis of removal efficiency

The pH value is one of the most important factors that control the COD adsorption from cheese whey wastewater. The effect of pH on the efficiency of COD adsorption from cheese whey wastewater by ZFA in the pH range of 2–12 was investigated and the results are shown in Fig. 5. Accordingly, the COD adsorption efficiency increased with the increase of the solution pH.

The PZC of the ZFA is 7.3. At lower pH values ($pH < pH_{PZC}$), the adsorbent had a positive charge. Moreover, cheese whey wastewater may be present in cationic forms. In

Table 1
RFA chemical composition by XRF

Composition	SiO_2	Al_2O	Fe_2O_3	CaO	MgO	LiO	SO_3	K_2O	Na_2O
Weight%	37/88	28/73	18.07	11.54	1.79	0.98	0.38	0.34	0.29

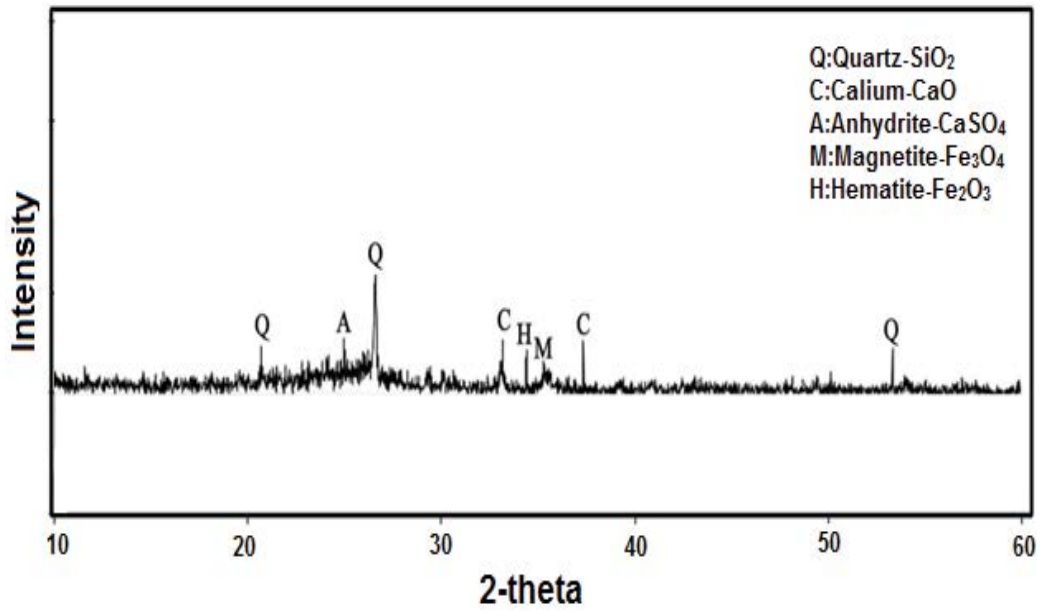

Fig. 1. XRD pattern of RFA.

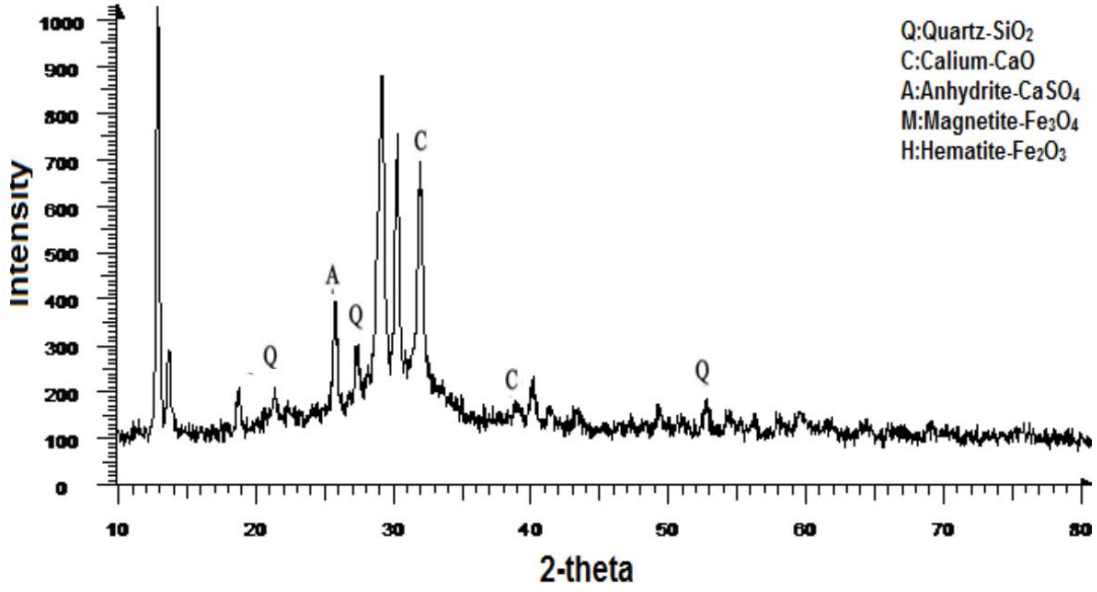

Fig. 2. XRD pattern of ZFA.

such conditions, cheese whey molecules have a low tendency to the absorbents. By increasing the pH value ($pH \geq pH_{PZC}$), cheese whey removal tends to change in inverse.

Consequently, the adsorbent had better performance in the neutral or low acidic milieu than the high acidic one. Low efficiency in low pH can be attributed to the H^+ ions presence in an acidic milieu which competes with COD for occupying active sites and then by occupying these sites decreases COD adsorption. Another effect of H^+ in the acidic milieu was the ionization of the adsorbent surface. During this phenomenon, the adsorbent surface became positively charged and had no affinity for the adsorption of COD [42]. Regarding the diagram, the optimum pH, at which the adsorption had maximum efficiency, was 11. Generally, it can be said adsorption of COD from cheese whey wastewater has better efficiency using ZFA.

3.4. Effect of contact time on removal efficiency

The contact time effect on the COD adsorption reaction is shown in Fig. 6. As can be seen in the diagram, as the process reached equilibrium, the adsorption efficiency increased with the increase of the contact time and did not change anymore afterwards. The reason is that, at the beginning of the reaction and as the contact time increased, the adsorbate had more time to move toward the adsorbent, and occupied the

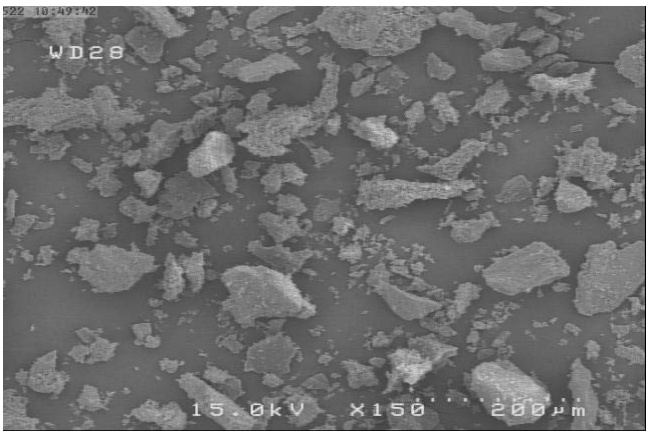

Fig. 3. SEM image of RFA surface.

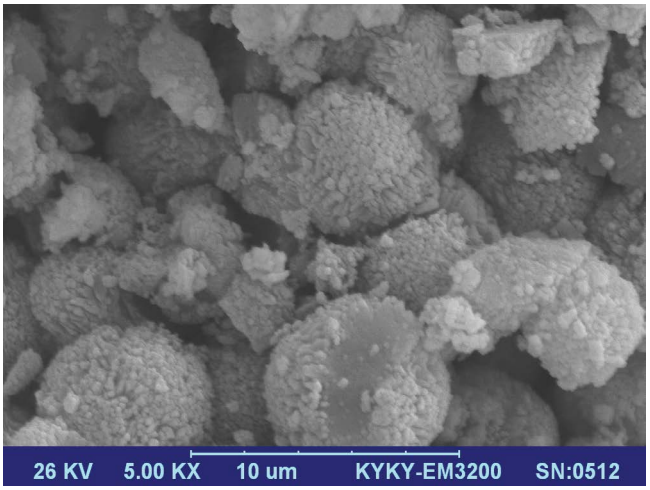

Fig. 4. SEM image of ZFA before adsorption process.

adsorbent active sites. But, when the process reached equilibrium, the adsorbent was saturated and increasing the contact time had no effect on the adsorption efficiency.

According to the diagram, the equilibrium contact time in this process is 20 min and adsorption efficiency at this time is 93.54%. Regard to this results, process contact time for other tests should be 20 min.

3.5. Adsorbent dosage effect on adsorption efficiency

To investigate the adsorbent dosage on COD adsorption efficiency, different amounts of adsorbents (0.05–0.45 g) in 50 mL of cheese whey wastewater with an initial concentration of 2,600 ppm of COD in optimum pH and contact time were used. Results are shown in Fig. 7. As can be seen, with the increase of the adsorbent amount from 0.05 to 0.4 g, the removal efficiency increased; but, it did not change after reaching the optimum amount of the adsorbent, that is, 0.4 g, which was used for further tests. The increase of the adsorption with the increase of the adsorbent amount can be justified by the point that, with the increase of the adsorbent amount, the available active sites for ion adsorption increased and, consequently, the

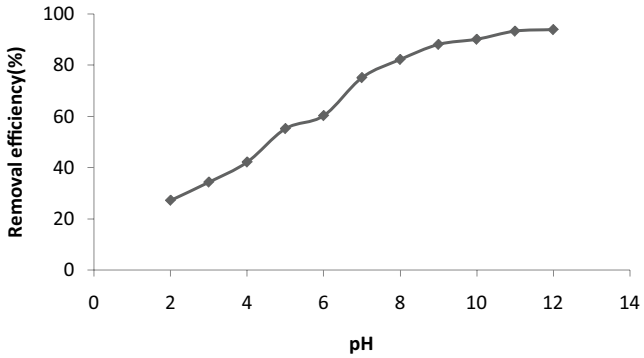

Fig. 5. Initial solution pH effect on COD adsorption efficiency.

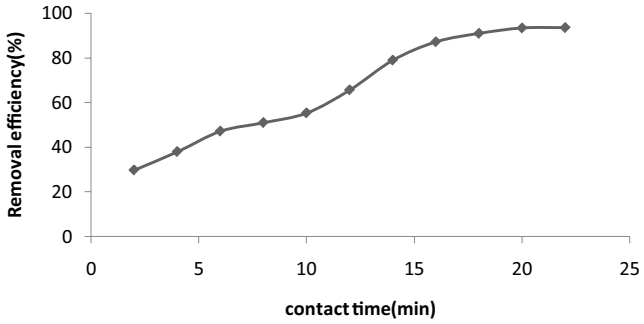

Fig. 6. Effect of contact time on COD adsorption efficiency on ZFA.

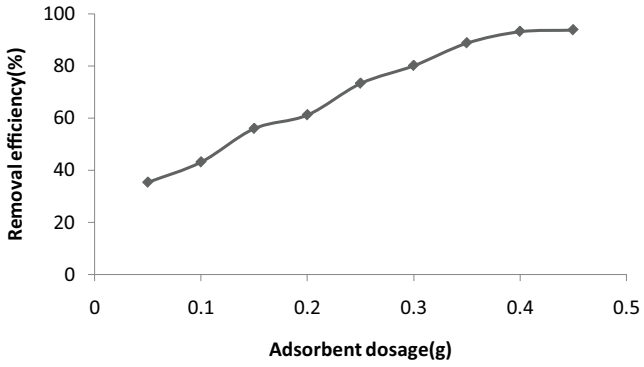

Fig. 7. Effect of adsorbent amount on COD adsorption efficiency.

adsorption efficiency increased. But, after reaching the optimum adsorbent amount, the solution reached equilibrium and adding more adsorbent had no more effects [17,45].

3.6. Analysis of adsorption kinetics

Most of the adsorption phenomena with different adsorbents depend on time. Kinetic consideration is very important for comprehending the reaction dynamics and the prediction of the adsorption conditions with time. Used models in this area are pseudo-first-order, pseudo-second-order, and Morris–Weber kinetic models. Morris–Weber equation is used to study the diffusion effect in the kinetic process.

Fig. 8a shows q_t diagram vs. $t^{1/2}$. If this diagram is linear, adsorption is controlled by diffusion and if this graph crosses the origin of coordinates, internal diffusion is the only limiting factor [46]. Also, internal diffusion constant, k_{id} (mg/g $h^{1/2}$), and C (mg/g) constant which is related to the boundary layer thickness can be obtained from slope and interception of q_t diagram vs. $t^{1/2}$, respectively. The calculated values of these constants and R^2 correlation coefficient are presented in Table 2.

As can be seen from Fig. 8a, diagram linearity shows that internal diffusion is one of the limiting steps of COD adsorption on ZFA. However, this step is not the only controlling step because the graph does not cross the origin of coordinates.

Fig. 8b shows a linear diagram of $\ln(q_e - q_t)$ vs. t. Pseudo-first-order kinetic model parameters are presented in Table 2. As it is shown, experimental data correlate slightly (R^2 = 0.7874) with a diagram. This issue shows that the

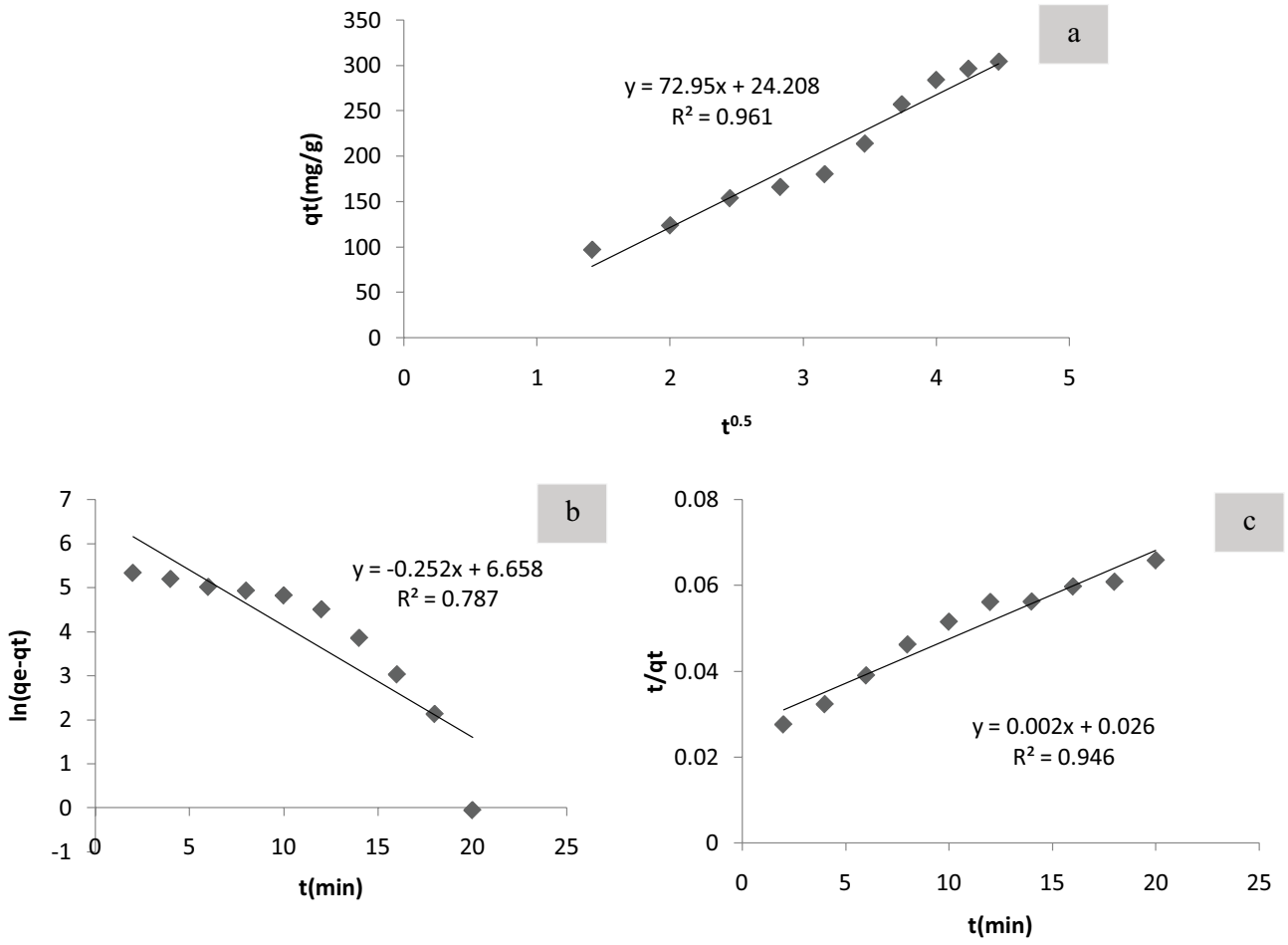

Fig. 8. Kinetic models for COD adsorption on ZFA (a) Morris–Weber, (b) pseudo-first-order, and (c) pseudo-second-order kinetics.

Table 2
Kinetics constants values for COD adsorption on ZFA

Kinetic model	Equation and corresponding diagram	Calculated constants		
Pseudo-second-order	$\frac{t}{q_t} = \frac{1}{k_2 q_e^2} + \frac{t}{q_e}$	k_2 (g/mg h)	q_e (mg/g)	R^2
	Plot: t/q_t vs. t	0.000165	471.1905	0.9465
Morris–Weber	$q_t = k_{id} t^{1/2} + C$	k_{id} (mg/g $h^{1/2}$)	C (mg/g)	R^2
	Plot: q_t vs. $t^{1/2}$	72.95	24.208	0.961

pseudo-first-order equation is not a good model to describe COD adsorption kinetics.

The pseudo-second-order kinetic model is based on the assumption that the limiting step can be a chemical adsorption reaction such as the electron exchange between the adsorbate and adsorption. Fig. 8c indicates the t/q_t vs. t linear diagram. Equilibrium capacity q_e (mg/g) and pseudo-second-order equation constant k_2 (g/mg h) are presented in Table 2.

As shown in Fig. 8c, the experimental data correlated well with the diagram (R^2 = 0.9465). This issue indicated that the pseudo-second-order equation is a suitable model for the kinetic description of the COD adsorption reaction on RFA.

By analyzing these three models, it became obvious that the experimental data correlated well with the pseudo-second-order equation. This issue shows that the pseudo-second-order kinetics model assumption rules COD adsorption on ZFA and the limiting step in this process is chemical adsorption reaction including electron exchange between adsorbate and adsorbent. In this regard, Katal et al. [47] found that, in the adsorption processes from the aqueous solutions by adsorbents, the pseudo-first-order equation only ruled when the adsorbate concentration in the aqueous solution was high; at the low concentrations, the adsorption was according to the pseudo-second-order equation.

Experimental data has also good agreement with Morris–Weber kinetic model and this agreement shows that another limiting step in this reaction is internal diffusion.

3.7. Analysis of adsorption isotherms

Generally, the adsorption isotherm models show the adsorbate quantity in equilibrium as a function of the adsorbate equilibrium concentration in the solution with a constant temperature. In this paper, four isotherm models have been investigated for the COD adsorption mechanism on ZFA and their results are presented in Fig. 9 and Table 3.

As can be seen in Fig. 9a, the experimental data correlated well with the Langmuir linear graph with a high correlation coefficient so it can be stated that the Langmuir isotherm is a suitable model for describing the mechanism of the COD adsorption on the ZFA mechanism. This demonstrates the Langmuir assumption ruling the homogenous distribution of the active sites on ZFA and the COD monolayer coverage on their surface [38]. The R_L value for adsorption by ZFA was 0.00000008. Both R_L values are between 0 and 1, and indicate that COD adsorption from cheese whey wastewater by ZFA is possible and favourable [48].

The experimental data correlated well and with a high correlation coefficient with the Freundlich and Temkin linear graphs. Therefore, it can be stated that these isotherms are also suitable for describing the mechanism of COD adsorption on ZFA. The calculated values of n are presented in Table 3. Both of these values were between 2 and 10 and indicated good adsorption characteristics, as well as favorable COD adsorption process from cheese whey wastewater by ZFA [48]. But, analyzing the Dubinin–Radushkevich isotherm model showed that the experimental data slightly correlated with the graph. Therefore, the Dubinin–Radushkevich isotherm model weakly described the COD adsorption mechanism on this adsorbent.

Eventually, comparison among these models showed that except Dubinin–Radushkevich rest of models have good agreement with experimental data. Moreover, constants calculated values of these isotherms indicated the possibility and favorability of COD adsorption reaction on ZFA.

3.8. Analyzing effect of temperature on removal efficiency

Temperature effect on COD removal from cheese whey wastewater were investigated at 25°C, 35°C, and 45°C. Tests were accomplished in previous optimum conditions. Results are presented in Table 4. As results indicate, in tests accomplished with adsorbent, an increase in temperature increases COD removal efficiency. However, this increase is not significant. To justify this case, it can be stated that with the increase of temperature, the boundary layer thickness around the adsorbent decreased, so the transportation of the adsorbate from the solution to the adsorbent active sites happened more easily and this increased the removal efficiency. Temperature increases could add to the available active sites for adsorption. Moreover, the increase in temperature increased the forces between the adsorbent and the adsorbate as well as the adjacent adsorbate intermolecular forces, because the COD adsorption from cheese whey wastewater was chemical adsorption. The positive effect of temperature on the removal efficiency showed that the COD adsorption reaction was endothermic [38].

3.9. Thermodynamics investigation

Thermodynamics of adsorption processes using data in Table 4 have been discussed and Gibbs free energy (ΔG°),

Table 3
Isotherms constants values for COD adsorption on ZFA

Isotherm model	Equation and corresponding diagram	Calculated constants		
Langmuir	$C_e/q_e = 1/q_0 K_L + C_e/q_0$	q_0 (mg/g)	K_L (L/mg)	R^2
	Plot: C_e/q_e vs. C_e	714.285	477.857	0.9592
Freundlich	$\log(q_e) = \log(K_F) + 1/n \log(C_e)$	n	K_F	R^2
	Plot: $\log(q_e)$ vs. $\log(C_e)$	3.084	49.35	0.9464
Temkin	$q_e = B \ln(K_T) + B \ln(C_e)$	B	K_T	R^2
	Plot: q_e vs. (C_e)	122.44	19.08	0.908

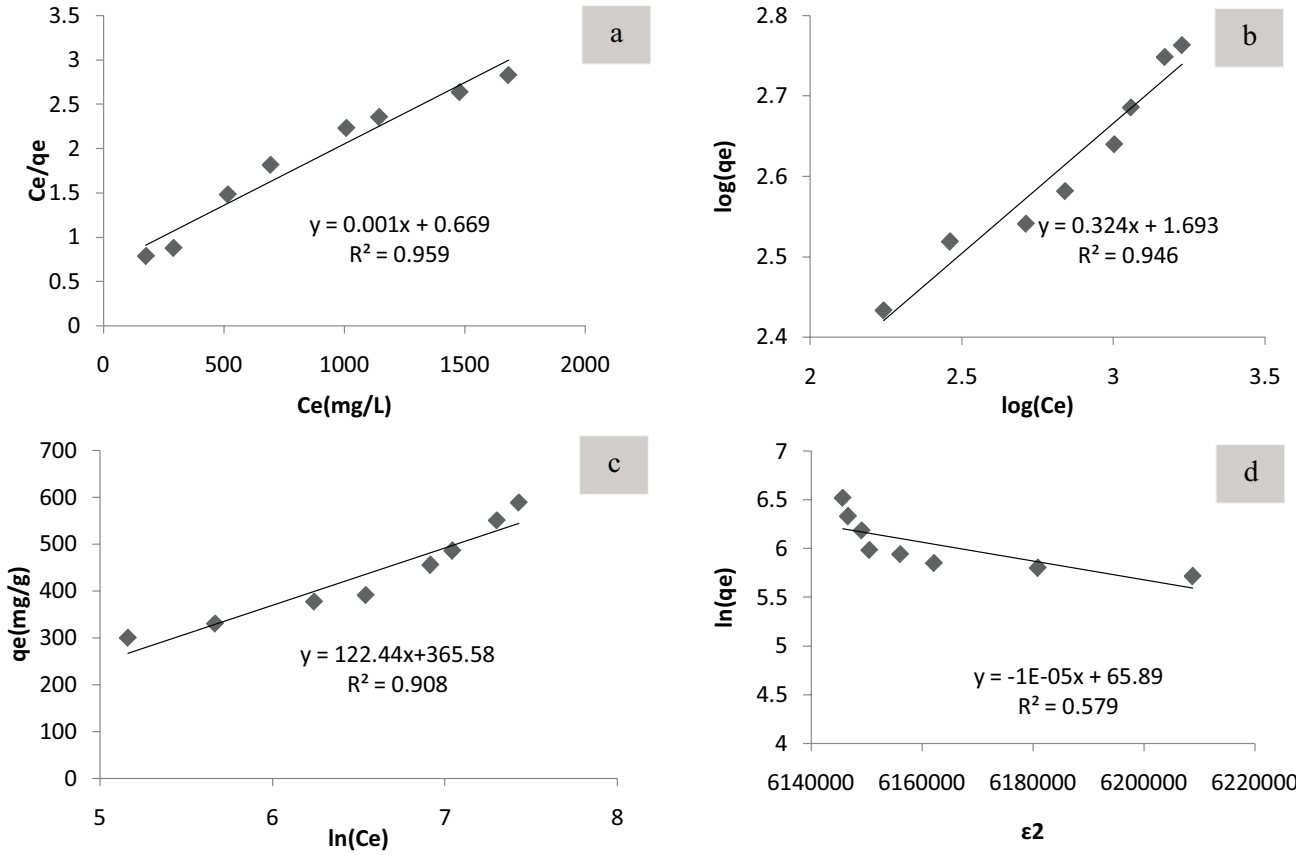

Fig. 9. Adsorption isotherms for COD adsorption on ZFA (a) Langmuir, (b) Freundlich, (c) Temkin, and (d) Dubinin–Radushkevich isotherm.

Table 4
Temperature effect on COD adsorption efficiency

Temperature (°C)	Removal efficiency %
25	93.3
35	95.1
45	96.8

enthalpy ($\Delta H°$), and entropy ($\Delta S°$) changes are calculated based on Eqs. (17)–(19):

$$K_c = \frac{F_e}{1-F} \tag{17}$$

$$\log K_c = \frac{-\Delta H°}{2.303RT} + \frac{-\Delta S°}{2.303R} \tag{18}$$

$$\Delta G° = -RT \ln K_c \tag{19}$$

$$\Delta G° = \Delta H° - T\Delta S° \tag{20}$$

In these equations, F_e is a fraction of COD which is adsorbed in equilibrium. R (J/k mol) is universal gas constant and T (K) is the absolute temperature.

The values of $\Delta H°$ and $\Delta S°$ were obtained from the slope and intercept of the $\log K_c$ vs. $1/T$ diagram. Values of $\Delta G°$ in three temperatures are calculated using Eq. (20). The calculated thermodynamic parameters are presented in Table 5. The negative values of $\Delta G°$ in Table 5 revealed that the adsorption by the adsorbent was a spontaneous process. As can be seen, the positive amount of $\Delta S°$ and the positive value of $\Delta H°$ represented that the process was endothermic with the increase of randomness at the solid-solution interface within the adsorption [49,50].

3.10. ZFA structure investigation after adsorption process by FTIR

ZFA structure by FTIR analysis, before and after COD adsorption from cheese whey wastewater is presented in Figs. 10a and b. By comparison of two figures, it is obvious that in ZFA structure FTIR analysis after the adsorption process no peak was observed that indicates adsorption is physical.

3.11. Morphology and chemical structure investigation of ZFA after adsorption by SEM

Fig. 11 shows ZFA surface morphology after the adsorption process. As can be seen, the ZFA structure has not changed during COD adsorption from the wastewater process.

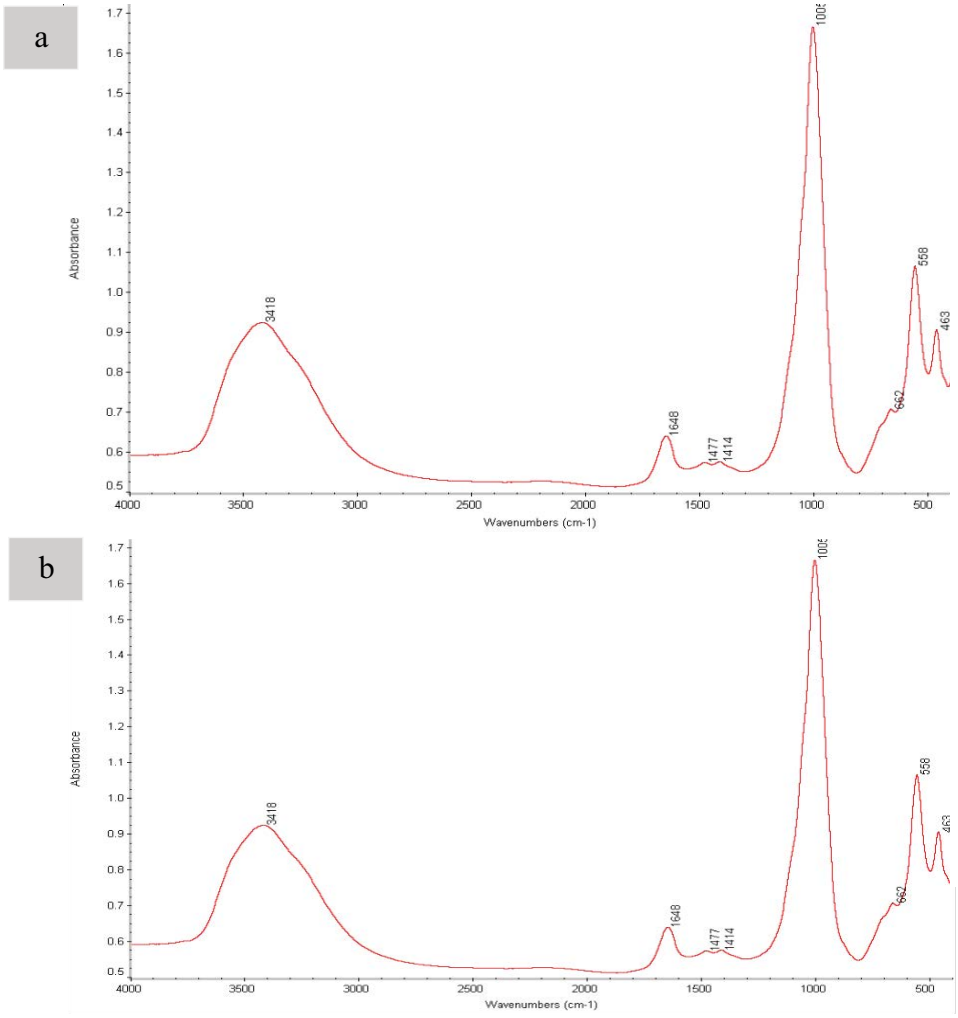

Fig. 10. FTIR spectrum of ZFA (a) before and (b) after adsorption.

Table 5
Values of thermodynamic parameters for COD adsorption on ZFA

$\Delta H°$ (kJ/mol)	$\Delta S°$ (kJ/mol)	T (°C)	$\Delta G°$ (kJ/mol)	R^2
		25	–6.525	
2.04	0.091	35	–7.3477	0.93
		45	–8.447	

4. Conclusion

In this paper, the ZFA synthesis from RFA by the two-stage process of alkaline melt-hydrothermal synthesis was reviewed and ZFA was used as the adsorbent in the batch tests of the COD removal from cheese whey wastewater. Results are as follows:

- Structural and characteristics investigation of raw RFA by XRF, XRD, and SEM analysis showed that used ash in this paper is type *F* and 84.68% of its weight is SiO_2, Al_2O_3, and Fe_2O_3. Main crystal phase in this ash is quartz (SiO_2) and its appearance is irregular and non-porous.
- In the COD adsorption tests by ZFA, the optimum pH, and contact time were 11 and 20 min, respectively. Optimum amount of adsorbent in COD adsorption

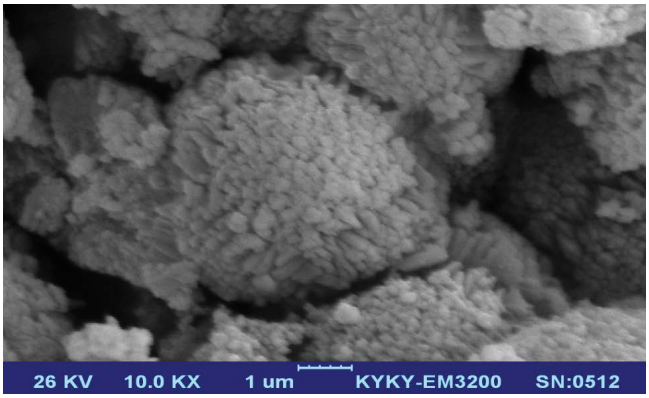

Fig. 11. SEM image of ZFA after adsorption process.

from cheese whey wastewater tests was 0.4 g in 50 mL of solution. Moreover, the analysis of the effect of temperature on the adsorption process in the 25°C–45°C range indicated that the increase in temperature had a positive effect on the removal efficiency of COD.

- Calculated values of thermodynamic parameters in COD adsorption process are: $\Delta H° = 2.04$ kJ/kmol, $\Delta S° = 0.091$ kJ/kmol, and $\Delta G°$ = –6.525, –7.3477, and –8.447 kJ/kmol. According to these values, COD adsorption reaction on ZFA is endothermic and spontaneous.
- Comparing the FTIR spectrum of ZFA before and after the COD adsorption reaction from cheese whey wastewater proved that the adsorption was physical. Moreover, the SEM image of ZFA after the adsorption revealed that the ZFA structure did not change during the COD adsorption from the cheese whey wastewater process.
- COD adsorption on ZFA reaction kinetics was studied and experimental data have the best agreement with pseudo-first-order and Morris–Weber model and Morris–Weber model can be stated that internal diffusion step is one of the controlling steps of this reaction.
- The Langmuir, Freundlich, Dubinin–Radushkevich, and Temkin models were studied for the COD adsorption mechanism on ZFA and, except for the Dubinin–Radushkevich model, all the other models were in good agreement with the experimental data. Moreover, the obtained values of these isotherm constants demonstrated the possibility and favorability of the COD adsorption reaction on ZFA.

References

[1] G. Munavalli, P. Saler, Treatment of dairy wastewater by water hyacinth, Water Sci. Technol., 59 (2009) 713–722.
[2] P. Malik, S. Saha, Oxidation of direct dyes with hydrogen peroxide using ferrous ion as catalyst, Sep. Purif. Technol., 31 (2003) 241–250.
[3] M. Koch, A. Yediler, D. Lienert, G. Insel, A. Kettrup, Ozonation of hydrolyzed azo dye reactive yellow 84 (CI), Chemosphere, 46 (2002) 109–113.
[4] T. Panswad, S. Wongchaisuwan, Mechanisms of dye wastewater colour removal by magnesium carbonate-hydrated basic, Water Sci. Technol., 18 (1986) 139–144.
[5] G. Ciardelli, L. Corsi, M. Marcucci, Membrane separation for wastewater reuse in the textile industry, Resour. Conserv. Recycl., 31 (2001) 189–197.
[6] M. Anbia, K. Mohammadi, Novel and efficient nanoporous adsorbent for dichromate ion and furfural removal from aqueous solutions, Asian J. Chem., 21 (2009) 3347–3354.
[7] M. Kamari, S. Shafiee, F. Salimi, C. Karami, Comparison of modified boehmite nanoplatelets and nanowires for dye removal from aqueous solution, Desal. Water Treat., 161 (2019) 304–314.
[8] A. Naghizadeh, M. Kamranifar, A.R. Yari, M.J. Mohammadi, Equilibrium and kinetics study of reactive dyes removal from aqueous solutions by bentonite nanoparticles, Desal. Water Treat., 97 (2017) 329–337.
[9] H. Rezaei, M.R. Narooie, R. Khosravi, M.J. Mohammadi, H. Sharafi, H. Biglari, Humic acid removal by electrocoagulation process from natural aqueous environments, Int. J. Electrochem. Sci., 13 (2018) 2379–2389.
[10] F. Salimi, H. Rahimi, C. Karami, Removal of methylene blue from water solution by modified nanogoethite by Cu, Desal. Water Treat., 137 (2019) 334–344.
[11] P. Veerakumar, T. Jeyapragasam, Surabhi, K. Salamalai, T. Maiyalagan, K.-C. Lin, Functionalized mesoporous carbon nanostructures for efficient removal of Eriochrome black-T from aqueous solution, J. Chem. Eng. Data, 64 (2019) 1305–1321.
[12] P.A. Ramalho, Degradation of Dyes with Microorganisms: Studies with Ascomycete Yeasts, University of Minho, 2005.
[13] A.R. Dinçer, Y. Güneş, N. Karakaya, Coal-based bottom ash (CBBA) waste material as adsorbent for removal of textile dyestuffs from aqueous solution, J. Hazard. Mater., 141 (2007) 529–535.
[14] Y. Dai, N. Zhang, C. Xing, Q. Cui, Q. Sun, The adsorption, regeneration and engineering applications of biochar for removal organic pollutants: a review, Chemosphere, 223 (2019) 12–27.
[15] S. Hokkanen, A. Bhatnagar, M. Sillanpää, A review on modification methods to cellulose-based adsorbents to improve adsorption capacity, Water Res., 91 (2016) 156–173.
[16] M. Kaykhaii, M. Sasani, S. Marghzari, Removal of dyes from the environment by adsorption process, Chem. Mater. Eng., 6 (2018) 31–35.
[17] F. Salimi, M. Eskandari, C. Karami, Investigation of methylene blue adsorption in wastewater using nano-zeolite modified with copper, Desal. Water Treat., 85 (2017) 206–214.
[18] R.S. Bowman, Applications of surfactant-modified zeolites to environmental remediation, Microporous Mesoporous Mater., 61 (2003) 43–56.
[19] P.J. Reeve, H.J. Fallowfield, Natural and surfactant modified zeolites: a review of their applications for water remediation with a focus on surfactant desorption and toxicity towards microorganisms, J. Environ. Manage., 205 (2018) 253–261.
[20] Y. Yaping, Z. Xiaoqiang, Q. Weilan, W. Mingwen, Synthesis of pure zeolites from supersaturated silicon and aluminum alkali extracts from fused coal fly ash, Fuel, 87 (2008) 1880–1886.
[21] C.A. Ríos R, C.D. Williams, C.L. Roberts, A comparative study of two methods for the synthesis of fly ash-based sodium and potassium type zeolites, Fuel, 88 (2009) 1403–1416.
[22] C. Belviso, F. Cavalcante, S. Fiore, Synthesis of zeolite from Italian coal fly ash: differences in crystallization temperature using seawater instead of distilled water, Waste Manage., 30 (2010) 839–847.
[23] A. Shoumkova, V. Stoyanova, Zeolites formation by hydrothermal alkali activation of coal fly ash from thermal power station "Maritsa 3", Bulgaria, Fuel, 103 (2013) 533–541.
[24] S.P. Kamble, P.A. Mangrulkar, A.K. Bansiwal, S.S. Rayalu, Adsorption of phenol and o-chlorophenol on surface altered fly ash based molecular sieves, Chem. Eng. J., 138 (2008) 73–83.
[25] M. Ahmaruzzaman, Adsorption of phenolic compounds on low-cost adsorbents: a review, Adv. Colloid Interface Sci., 143 (2008) 48–67.
[26] D. Smiljanić, B. de Gennaro, F. Izzo, A. Langella, A. Daković, C. Germinario, G.E. Rottinghaus, M. Spasojević, M. Mercurio, Removal of emerging contaminants from water by zeolite-rich composites: a first approach aiming at diclofenac and ketoprofen, Microporous Mesoporous Mater., 298 (2020) 1–12, doi: 10.1016/j.micromeso.2020.110057.
[27] J.A. Oliveira, F.A. Cunha, L.A. Ruotolo, Synthesis of zeolite from sugarcane bagasse fly ash and its application as a low-cost adsorbent to remove heavy metals, J. Cleaner Prod., 229 (2019) 956–963.
[28] X. Deng, L. Lü, H. Li, F. Luo, The adsorption properties of Pb(II) and Cd(II) on functionalized graphene prepared by electrolysis method, J. Hazard. Mater., 183 (2010) 923–930.
[29] R. Leyva-Ramos, L. Bernal-Jacome, I. Acosta-Rodriguez, Adsorption of cadmium(II) from aqueous solution on natural and oxidized corncob, Sep. Purif. Technol., 45 (2005) 41–49.
[30] C. Moreno-Castilla, M. Lopez-Ramon, F. Carrasco-Marın, Changes in surface chemistry of activated carbons by wet oxidation, Carbon, 38 (2000) 1995–2001.
[31] D.D. Do, Adsorption Analysis: Equilibria and Kinetics, Imperial College Press, London, 1998.
[32] T.D. Reynolds, P.A.C. Richards, Unit Operations and Processes in Environmental Engineering, PWS Publishing Company, Boston, MA, 1995.
[33] M. Temkin, V. Pyzhev, Kinetics of ammonia synthesis on promoted iron catalysts, Acta Physiochim. URSS, 12 (1940) 217–222.

[34] A. Günay, E. Arslankaya, I. Tosun, Lead removal from aqueous solution by natural and pretreated clinoptilolite: adsorption equilibrium and kinetics, J. Hazard. Mater., 146 (2007) 362–371.
[35] A. Dąbrowski, Adsorption—from theory to practice, Adv. Colloid Interface Sci., 93 (2001) 135–224.
[36] M. Dubinin, The equation of the characteristic curve of activated charcoal, Dokl. Akad. Nauk. SSSR, 55 (1947) 327–329.
[37] M. Jiménez-Cedillo, M. Olguín, C. Fall, Adsorption kinetic of arsenates as water pollutant on iron, manganese and iron–manganese-modified clinoptilolite-rich tuffs, J. Hazard. Mater., 163 (2009) 939–945.
[38] W.J. Weber, J.C. Morris, Kinetics of adsorption on carbon from solution, J. Sanitary Eng. Div., 89 (1963) 31–60.
[39] M. Harja, G. Buema, D.-M. Sutiman, C. Munteanu, D. Bucur, Low cost adsorbents obtained from ash for copper removal, Korean J. Chem. Eng., 29 (2012) 1735–1744.
[40] R.L. Davison, D.F. Natusch, J.R. Wallace, C.A. Evans Jr., Trace elements in fly ash. Dependence of concentration on particle size, Environ. Sci. Technol., 8 (1974) 1107–1113.
[41] G.I. McCarthy, X-ray powder diffraction for studying the mineralogy of fly ash, MRS Online Proc. Libr. Arch., 113 (1987) 75–86, doi: 10.1557/PROC-113-75.
[42] R. Katal, E. Hasani, M. Farnam, M.S. Baei, M.A. Ghayyem, Charcoal ash as an adsorbent for Ni(II) adsorption and its application for wastewater treatment, J. Chem. Eng. Data, 57 (2012) 374–383.
[43] S.G. Thoma, T.M. Nenoff, A novel synthesis of zeolite W using organometallic precursors, Microporous Mesoporous Mater., 34 (2000) 301–306.
[44] S.N. Azizi, N. Asemi, The effect of ultrasonic and microwave-assisted aging on the synthesis of zeolite p from Iranian perlite using Box–Behnken experimental design, Chem. Eng. Commun., 201 (2014) 909–925.
[45] M. Mohamadi, F. Salimi, S. Sadeghi, Reduction of oil, COD and turbidity of Kermanshah oil refinery effluent using modified nano-zeolite by bismuth and iron, Desal. Water Treat., 97 (2017) 151–157.
[46] S. Lagergren, Zur theorie der sogenannten adsorption gelöster stoffe, K. Sven. Vetenskapsakad. Handl., 24 (1898) 1–39.
[47] R. Katal, E. Hasani, M. Farnam, M.S. Baei, M.A. Ghayyem, Charcoal ash as an adsorbent for Ni(II) adsorption and its application for wastewater treatment, J. Chem. Eng. Data, 57 (2012) 374–383.
[48] L. Yu, Q. Zhong, Preparation of adsorbents made from sewage sludges for adsorption of organic materials from wastewater, J. Hazard. Mater., 137 (2006) 359–366.
[49] G. Sheng, J. Li, D. Shao, J. Hu, C. Chen, Y. Chen, X. Wang, Adsorption of copper(II) on multiwalled carbon nanotubes in the absence and presence of humic or fulvic acids, J. Hazard. Mater., 178 (2010) 333–340.
[50] G. Mckay, Use of Adsorbents for the Removal of Pollutants from Wastewater, CRC Press, Boca Raton, FL, 1995.